Study of the Reaction $\pi^- p \rightarrow \pi^+ \pi^- n$ at an Incident Energy of 870 MeV

M. BANNER, J. F. DETOEUF, M. L. FAYOUX, J. L. HAMEL, AND J. ZSEMBERY
Département de Physique des Particules Elémentaires, Centre d'Etudes Nucléaires de Saclay, Gif-sur-Yvette, g1-France

AND

J. CHEZE AND J. TEIGER
Faculté des Sciences de Caen, Caen, France

(Received 7 August 1967)

In the reaction $\pi^- p \rightarrow \pi^+ \pi^- n$, we have measured the π^+ momentum spectrum at various angles, from which the distributions $(d^2\sigma/dMd\Omega)^*$ of the $\pi^- n$ system have been deduced. These distributions are compared with those obtained from a phenomenological model. This comparison allows a determination of the amplitude of the inelastic waves. It is found that the resonant waves D_{15} and F_{15} are not strongly coupled to the channel $\Delta(1238)+\pi$.

I. INTRODUCTION

THE study of the elastic reactions $\pi^\pm p \rightarrow \pi^\pm p$ has shown that the partial waves D_{15}, F_{15} are resonating around an incident pion kinetic energy of 870 MeV.[1] These waves are strongly absorbed and give an important contribution to the inelastic processes

$$\begin{aligned} \pi^- p &\rightarrow \pi^- \pi^+ n \\ &\rightarrow \pi^- \pi^0 p \\ &\rightarrow \pi^0 \pi^0 n . \end{aligned}$$

The channel $\pi^-\pi^+ n$ has a cross section of 12 mb, to be compared with a total inelastic cross section of 22 mb. It is thus sufficiently prolific to show the effects of the D_{15} and F_{15} partial waves. In order to study the contribution of resonances to the inelastic channels, one has to decompose the transition amplitude for the reactions into partial waves[2] and compare the results of the calculations with the experimental angular distributions and mass spectra. In this way, one hopes to determine the relative weights of the inelastic partial waves for the chosen incident energy.

Deler and Valladas[2] have given a partial-wave expansion of the transition amplitude for a three-body final-state reaction like $\pi+N \rightarrow 1+2+3$. They assume that the reaction takes place as a two-body process, producing a resonance C^*, which subsequently decays:

$$\pi+N \rightarrow 1+C^* \searrow 2+3.$$

In the case of the reaction $\pi^- p \rightarrow \pi^- \pi^+ n$, the three ways of associating the final-state particles, $\pi^- n$, $\pi^+ n$, $\pi^-\pi^+$, allow the resonance C^* to be the isobar $\Delta(1238)$, or a π-π resonance with isospin and spin zero, with a mass and a width to be determined.

We have measured the momentum spectrum of the π^+ at various angles and obtained the differential cross section $d^2\sigma/dMd\Omega$ (M = invariant mass of the subsystem $\pi^- n$) in the over-all center-of-mass (c.m.) system.

The calculation of $d^2\sigma/dMd\Omega$ takes account of (a) the interferences due to the simultaneous presence of the three possible modes of associating the final-state particles; (b) the interference due to the two possible total isospin values in the initial state, $I=\frac{1}{2}$ and $I=\frac{3}{2}$; and (c) the interference between the various partial waves.

II. EXPERIMENTAL EQUIPMENT

The method consists in determining the momentum p_{π^+} and the angle θ_{π^+} with respect to the direction of the incident pion. Knowing the incident pion momentum, one computes the mass M_X to be associated with the "particle" X in the reaction $\pi^- + p \rightarrow \pi^+ + X$. The momentum p_{π^+} is determined by the deviation of the π^+ trajectory in a known magnetic field.

A. Apparatus

The general layout of the experiment is shown in Fig. 1. A_1 and A_2 are two spark chambers defining the incident pion trajectory. The spark chambers B_1 and B_2 detect the secondary particle after scattering in the target and determine its entrance angle in the magnet. The spark chamber C determines its position and angle

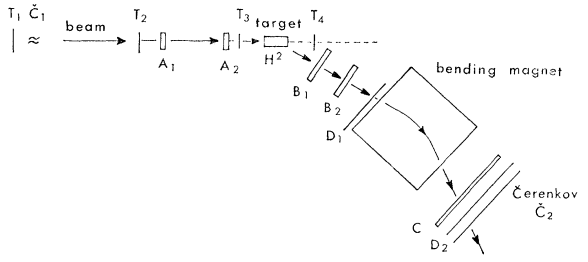

FIG. 1. The beam is defined with the scintillation counters T. A, B, and C are spark chambers. The D_1 and D_2 counters are used to trigger the electronics.

[1] P. Bareyre, C. Bricman, A. V. Stirling, and G. Villet, Phys. Letters **18**, 342 (1965).
[2] B. Deler and G. Valladas, Nuovo Cimento **45**, 559 (1966).

at the exit of the magnet. A scintillation counter system selects the events for which the chambers are triggered.

The triggering conditions are the incident particle is a pion, the particle has interacted in the target, and the scattered particle has crossed the magnet.

Two orthogonal views are taken for each chamber. A mirror system brings all the views on a single picture. The stand supporting the magnet and the spark chambers B_1, B_2, and C can rotate about the target. Each position of this spectrometer covers an angular region of 12° in the laboratory.

The incident pions are momentum analyzed and focused on the hydrogen target by a double-focusing beam transport system. The liquid-hydrogen target has a diameter of 10 cm and a length of 34.8 cm.

B. Electronics

In order to avoid normalization errors, the incident pions are counted only when the apparatus is able to accept the events. After triggering the spark chambers and the camera, an electronic gate stops the counting during the dead time.

C. Spark Chambers

The chambers A_1 and A_2, of identical construction, are placed 50 cm apart. The same is true for the chambers B_1 and B_2. The electrodes consist of aluminum foils of 0.3 mm thickness for the chamber A and 0.5 mm for the chambers B and C.

D. Optics and Photographs

The reconstruction of the trajectories in each chamber is obtained by projecting the sparks onto two orthogonal fiducial planes. These planes consist of Plexiglas plates placed on the chambers. A flash placed at one end of the fiducial plate allows a picture of the fiducial lattice to be taken. A typical picture is reproduced on Fig. 2. Since the films are scanned by an automatized device, the fiducial grids have to be of a special shape; straight lines are engraved to materialize the middle of the gaps of the chambers. The sparks sit astride these lines. One out of three gaps is not used to get sparks but, instead, fiducial marks are engraved every 5 cm on the corresponding straight lines. These marks are used for the calibration of the optical aberrations of the cameras and projection apparatus.

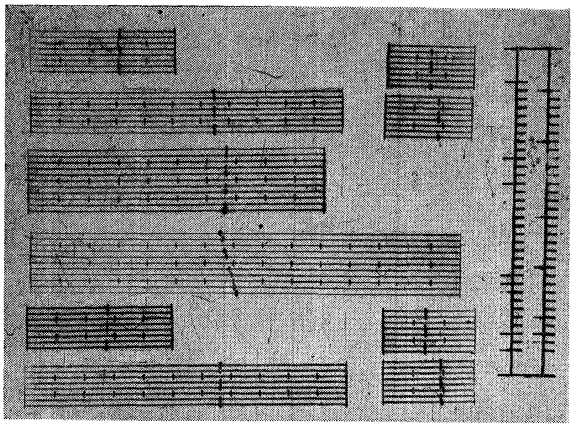

FIG. 2. Sample picture showing the data box and the fiducial marks followed by the flying spot.

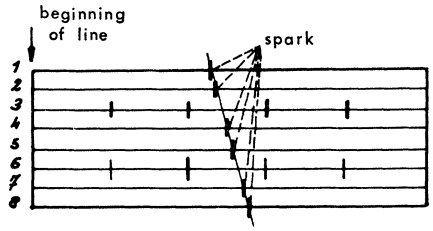

FIG. 3. Projection of the sparks belonging to a track, together with the fiducial marks. The spark positions are measured with respect to the beginning of a line.

III. RESULTS

The angular distribution of the missing-mass spectrum is given by the expression

$$\frac{d^2\sigma}{dM d\Omega}\frac{\text{mb}}{\text{sr MeV}}=\frac{N_{\text{ev}}}{N_{\text{inc}}}\times\frac{1}{N\rho l}\times\frac{1}{\Delta M\Delta\Omega}. \quad (1)$$

The four-body reaction being negligible,[3] Eq. (1) represents the cross section of the $\pi^- n$ system in the reaction $\pi^- p \to \pi^+ \pi^- n$. The angular distribution is thus given in the over-all c. m. system, with the following definitions in (1): N_{ev} is the number of events of the type $\pi^- p \to \pi^+ + (\pi^- n)$, such that the mass of $(\pi^- n)$ is equal to $M \pm \frac{1}{2}\Delta M$, and the cosine of the emission angle $\cos\theta \pm \frac{1}{2}\Delta \cos\theta$, where θ is the angle between the incident pion direction and the $(\pi^- n)$ direction in the over-all c.m. system. N_{inc} is the number of incident pions; N is the Avogadro number; ρ is the density of liquid hydrogen; l is the target length; $\Delta\Omega$ is the solid angle of the magnet seen from the target, transformed to the over-all c.m. system, for the events satisfying the selection criterion (N_{ev}).

The following three subsections will be concerned with the determination of the number of events, the calculation of the solid angle, and the measurement of the corresponding number of incident pions.

A. Determination of the Number of Events

The knowledge of the type of an event requires the determination of the π^+ momentum. The position of the sparks on a photograph is obtained by means of an automatic scanning apparatus.[4] In order to obtain the

[3] J. P. Merlo and G. Valladas, Proc. Roy. Soc. (London) A289, 489 (1966).

[4] M. Goldwasser, J. C. Michau, and J. Mullie, IEEE Trans. Nucl. Sci. NS-12, 73 (1965).

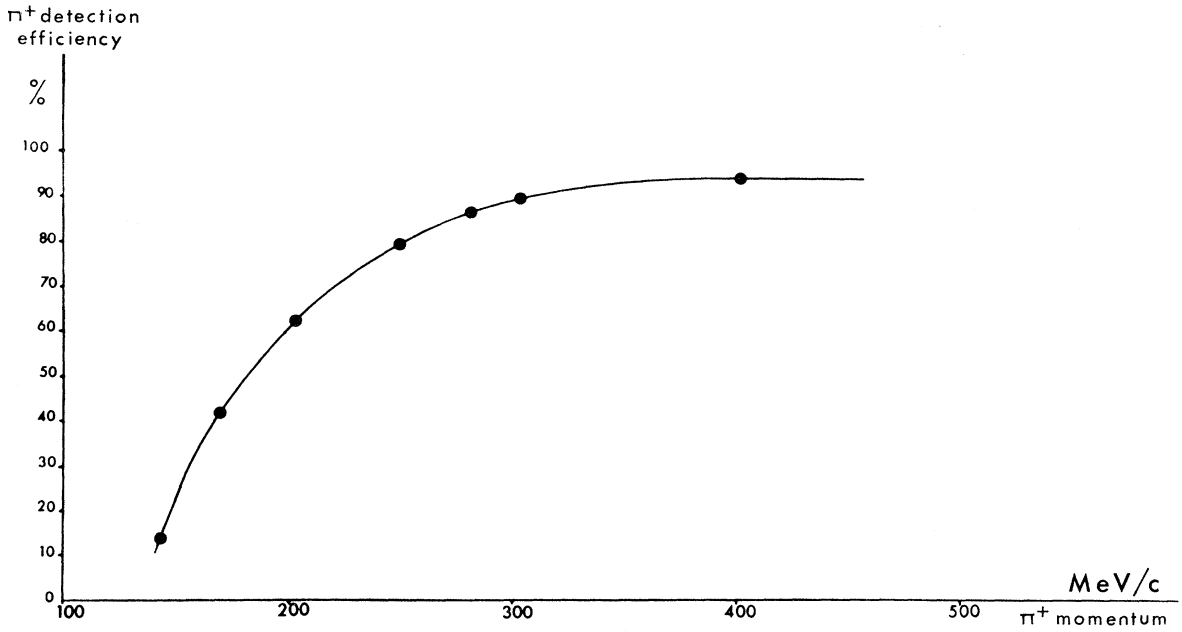

FIG. 4. π^+ detection efficiency of the Čerenkov counter C_2 as a function of the π^+ momentum. This Čerenkov counter is used to distinguish π^+ from protons.

coordinates of a spark, it is sufficient to measure its distance from the beginning of the fiducial line (Fig. 3). After the scanning of a photograph, all the information is transferred onto a magnetic tape. The data are subsequently processed using an IBM 7094. The analysis program computes the direction of the incident pion, the direction of the scattered particle, and its momentum, using the known magnetic field in the spectrometer magnet. It also requires the interaction point to be in the target.

B. Solid-Angle Calculation

The solid angle $\Delta\Omega$ is calculated by a Monte Carlo method. The incident particle direction is generated with a probability law consistent with the experimental distribution of the beam. The interaction point in the target is chosen at random.

C. Measurement of the Number of Incident Pions

The number of incident pions is given by the counting in the telescope $T_1\bar{C}_1T_2T_3$ (Fig. 1). At the beginning of the experiment, the beam contamination by muons was measured by a gas Čerenkov counter placed at the target position.

The experimental results are corrected for the following effects: (a) rescattering of the π^+ in the target, (b) interaction of the π^+ in the air and the counters, (c) π^+ decay in the analyzing magnet, (d) efficiency of the measuring apparatus, and (e) efficiency of the Čerenkov counter C_2.

Corrections (a), (b), and (c) are computed by a Monte Carlo method. Correction (d) is due to the fact that the scanning apparatus may miss a track if the sparks are not sufficiently contrasted. A manual check allows determining the number of π^+ lost in this way. On the average, the efficiency of the apparatus varies between 97 and 100%. As far as correction (e) is concerned, we remark that the counter C_2 is used to distinguish the π^+ from protons. About 12% of the protons coming from the reactions $\pi^-p \rightarrow \pi^-p$ and $\pi^-p \rightarrow \pi^-\pi^0p$ are counted in the Čerenkov counter C_2. On the other hand, the efficiency of this counter for counting the π^+'s varies with the momentum of the pions. Figure 4 shows the efficiency of the counter C_2 for the π^+'s as a function of the π^+ momentum.

D. Experimental Results

The distributions $(d^2\sigma/dMd\Omega)^*$ are given in Table I. (The asterisk indicates that the over-all c.m. system is used.) In addition to $(d^2\sigma/dMd\Omega)^*$ and its corresponding statistical error, the cosine of the emission angle of the particle X is also given. The first line of this table gives, for each column, the average value of the cosines of the corresponding column. The information contained in Table I is given in a different way in Table II. For each measured angle, the mass spectrum $(d^2\sigma/dMd\Omega)^*$ (Table I) is integrated with respect to the variable M (mass of the system π^-n) in mass bands of 50 MeV. One thus obtains the angular distributions $(d\sigma/d\Omega)_K^*$ for seven values of M.

The values of M are taken in the middle of the interval (K): 1.125, 1.175, 1.225, $\cdots$, 1.425 GeV. These distributions can be considered as the angular distribu-

TABLE I. Angle-mass distributions $(d^2\sigma/dMd\Omega)^*$ of the π^-n system in the over-all c.m. system. The average value of the cosines of the emission angle of the π^-n system is given in the first line. Each entry contains the cosine of the emission angle $\theta^*_{(\pi^-n)}$ of the (π^-n) system and below it the differential cross section $(d^2\sigma/dMd\Omega)^*$.

$M_{(\pi^-n)}$ (MeV) \ $\langle\cos\theta^*_{(\pi^-n)}\rangle_{av}$	-0.92 ± 0.04	-0.78 ± 0.04	-0.531 ± 0.025	-0.17 ± 0.05	0.147 ± 0.04	0.4066 ± 0.06	0.59 ± 0.025	0.752 ± 0.02	0.843 ± 0.016
1125.5	-0.89	-0.76	-0.50	-0.175	0.14	0.385	0.57	0.735	0.835
	0.30 ± 0.12	0.32 ± 0.08	0.29 ± 0.11	0.21 ± 0.13	0.21 ± 0.08	0.37 ± 0.15	0.33 ± 0.14	0.83 ± 0.32	0.49 ± 0.25
1137.5	-0.89	-0.76	-0.50	-0.175	0.14	0.385	0.57	0.735	0.835
	0.86 ± 0.26	0.64 ± 0.18	0.433 ± 0.09	0.29 ± 0.09	0.55 ± 0.14	0.63 ± 0.16	1.23 ± 0.35	1.25 ± 0.50	0.95 ± 0.47
1162.5	-0.90	-0.75	-0.53	-0.16	0.13	0.405	0.57	0.75	0.850
	1.45 ± 0.30	1.07 ± 0.20	1.07 ± 0.21	0.85 ± 0.20	1.26 ± 0.26	1.94 ± 0.56	1.35 ± 0.31	1.26 ± 0.66	1.25 ± 0.44
1187.5	-0.90	-0.75	-0.53	-0.16	0.13	0.405	0.57	0.75	0.850
	2.10 ± 0.42	1.71 ± 0.20	1.83 ± 0.21	0.91 ± 0.18	2.06 ± 0.40	2.18 ± 0.35	2.73 ± 0.43	2.57 ± 0.46	1.88 ± 0.52
1212.5	-0.90	-0.76	-0.51	-0.14	0.13	0.385	0.565	0.745	0.847
	3.02 ± 0.33	3.34 ± 0.36	2.22 ± 0.26	1.46 ± 0.26	2.06 ± 0.40	3.20 ± 0.41	3.87 ± 0.56	4.19 ± 1	2.75 ± 0.50
1237.5	-0.90	-0.76	-0.51	-0.14	0.13	0.385	0.565	0.745	0.847
	4.10 ± 0.55	3.34 ± 0.36	3.09 ± 0.30	2.01 ± 0.29	3.07 ± 0.40	4.07 ± 0.52	4.92 ± 0.56	4.36 ± 0.60	3.65 ± 0.64
1262.5	-0.915	-0.78	-0.52	-0.18	0.125	0.40	0.585	0.75	0.845
	3.60 ± 0.49	3.73 ± 0.40	2.81 ± 0.30	2.29 ± 0.32	2.58 ± 0.32	4.61 ± 0.54	4.01 ± 0.73	4.68 ± 0.60	2.34 ± 0.93
1287.5	-0.915	-0.78	-0.52	-0.18	0.125	0.40	0.585	0.75	0.845
	3.22 ± 0.49	3.42 ± 0.35	2.98 ± 0.30	2.10 ± 0.32	1.94 ± 0.32	2.83 ± 0.43	3.42 ± 0.44	2.86 ± 0.52	2.86 ± 0.60
1312.5	-0.92	-0.765	-0.555	-0.20	0.15	0.40	0.575	0.75	0.833
	3.46 ± 0.56	2.76 ± 0.31	3.24 ± 0.30	1.33 ± 0.24	2.01 ± 0.31	2.22 ± 0.43	3.48 ± 0.42	2.06 ± 0.44	3.36 ± 1.9
1337.5	-0.92	-0.765	-0.555	-0.20	0.15	0.405	0.575	0.75	0.833
	3.81 ± 0.50	3.50 ± 0.43	2.44 ± 0.25	1.39 ± 0.24	1.79 ± 0.34	2.22 ± 0.43	3.21 ± 0.42	2.74 ± 0.64	2.24 ± 0.43
1362.5	-0.94	-0.79	-0.555	-0.205	0.15	0.41	0.60	0.76	0.84
	3.31 ± 0.42	3.25 ± 0.37	2.28 ± 0.25	1.46 ± 0.26	1.89 ± 0.34	2.70 ± 0.49	2.60 ± 0.44	2.60 ± 0.50	2.06 ± 0.63
1387.5	-0.94	-0.79	-0.555	-0.205	0.15	0.41	0.60	0.76	0.84
	3.45 ± 0.58	2.46 ± 0.29	2.02 ± 0.36	1.46 ± 0.26	1.07 ± 0.31	2.78 ± 0.49	2.60 ± 0.44	3.36 ± 1.60	2.06 ± 0.63
1412.5	-0.937	-0.81	-0.55	-0.194	0.175	0.42	0.615	0.775	0.867
	2.36 ± 0.58	2.14 ± 0.34	1.97 ± 0.26	1.48 ± 0.26	2.11 ± 0.53	2.29 ± 0.41	3.0 ± 0.44	3.36 ± 1.21	1.88 ± 0.72
1437.5	-0.937	-0.81	-0.55	-0.194	0.175	0.42	0.615	0.775	0.867
	2.59 ± 0.41	2.24 ± 0.30	2.10 ± 0.30	1.21 ± 0.25	1.52 ± 0.37	2.79 ± 0.51	2.56 ± 1	2.55 ± 0.78	
1462.5	-0.945	-0.83	-0.55	-0.125	0.205	0.48	0.66		
	2.17 ± 0.64	1.78 ± 0.27	2.10 ± 0.37	1.50 ± 0.50	0.28 ± 0.12	2.49 ± 0.40	1.34 ± 0.43		
1487.5	-0.977	-0.82	-0.53	-0.10	0.34	0.51			
	2.20 ± 1.36	1.41 ± 0.28	2.70 ± 0.70	1.03 ± 0.51					

TABLE II. Angular distributions $(d\sigma/d\Omega)_K^*$, in the over-all c.m. system, for the mass value $M_{(\pi^-n)}$ of the (π^-n) system indicated in the first column. These angular distributions have been obtained by integrating the distributions $(d^2\sigma/dMd\Omega)^*$ of Table I. The average value of the cosine of the emission angle $\theta^*_{(\pi^-n)}$ is also given in each entry.

$M_{(\pi^-n)}$ (MeV)									
1125	-0.89	-0.76	-0.50	-0.175	0.14	0.385	0.57	0.735	0.835
	0.029 ± 0.007	0.024 ± 0.004	0.018 ± 0.003	0.013 ± 0.003	0.019 ± 0.004	0.025 ± 0.004	0.039 ± 0.007	0.052 ± 0.01	0.036 ± 0.01
1175	-0.90	-0.75	-0.53	-0.16	0.13	0.405	0.57	0.75	0.85
	0.089 ± 0.01	0.07 ± 0.005	0.073 ± 0.007	0.044 ± 0.007	0.083 ± 0.01	0.103 ± 0.01	0.102 ± 0.01	0.096 ± 0.01	0.078 ± 0.01
1225	-0.90	-0.76	-0.51	-0.14	0.13	0.385	0.565	0.745	0.847
	0.18 ± 0.07	0.167 ± 0.02	0.133 ± 0.01	0.087 ± 0.01	0.128 ± 0.01	0.182 ± 0.01	0.22 ± 0.01	0.214 ± 0.02	0.160 ± 0.04
1275	-0.915	-0.78	-0.52	-0.18	0.125	0.4	0.585	0.75	0.845
	0.17 ± 0.01	0.179 ± 0.01	0.145 ± 0.01	0.110 ± 0.01	0.113 ± 0.01	0.186 ± 0.01	0.186 ± 0.01	0.189 ± 0.02	0.13 ± 0.02
1325	-0.92	-0.765	-0.535	-0.20	0.15	0.405	0.575	0.75	0.833
	0.182 ± 0.01	0.16 ± 0.01	0.142 ± 0.009	0.068 ± 0.008	0.095 ± 0.01	0.111 ± 0.01	0.167 ± 0.01	0.12 ± 0.02	0.14 ± 0.05
1375	-0.94	-0.79	-0.555	-0.205	0.15	0.41	0.560	0.76	0.840
	0.171 ± 0.01	0.149 ± 0.01	0.109 ± 0.009	0.073 ± 0.009	0.074 ± 0.01	0.137 ± 0.01	0.13 ± 0.01	0.152 ± 0.03	0.103 ± 0.02
1425	-0.937	-0.81	-0.55	-0.194	0.175	0.42	0.615	0.775	0.867
	0.124 ± 0.01	0.110 ± 0.01	0.103 ± 0.008	0.067 ± 0.09	0.091 ± 0.01	0.127 ± 0.01	0.139 ± 0.01	0.152 ± 0.03	0.094 ± 0.02

TABLE III. Coefficients A_{L_1K} of the expansion in Legendre polynomials $P_{(L_1-1)}(\cos\theta^*_{(\pi^-n)})$ of the angular distributions of Table II. $F=\chi^2$/number of degrees of freedom; A_{1K} is the coefficient corresponding to the zero-order polynomial.

$M_{(\pi^-n)}$ (MeV)		A_1 (mb/sr)	A_2/A_1	A_3/A_1	A_4/A_1	A_5/A_1	A_6/A_1	F
1125	$K=1$	0.0266 ± 0.002	0.498 ± 0.09	0.794 ± 0.119	0 ± 0.1	0 ± 0.15	0 ± 0.3	0.32
1175	$K=2$	0.0739 ± 0.007	0.138 ± 0.125	0.026 ± 0.194	-0.561 ± 0.21	-0.432 ± 0.23	0 ± 0.36	1.6
1225	$K=3$	0.1489 ± 0.007	0.107 ± 0.10	0.226 ± 0.13	-0.51 ± 0.146	-0.565 ± 0.147	0 ± 0.09	0.16
1275	$K=4$	0.1437 ± 0.007	-0.054 ± 0.059	0.105 ± 0.085	-0.377 ± 0.092	-0.544 ± 0.1	0 ± 0.15	0.57
1325	$K=5$	0.1163 ± 0.012	-0.243 ± 0.15	0.299 ± 0.22	-0.47 ± 0.23	-0.62 ± 0.24	0 ± 0.35	1.5
1375	$K=6$	0.1070 ± 0.006	-0.131 ± 0.083	0.364 ± 0.12	-0.460 ± 0.14	-0.400 ± 0.14	0 ± 0.18	0.86
1425	$K=7$	0.1009 ± 0.006	0.044 ± 0.06	0.164 ± 0.09	-0.430 ± 0.1	-0.508 ± 0.11	0 ± 0.15	0.50

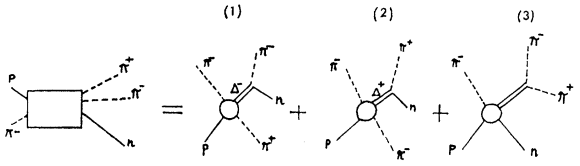

FIG. 5. The scattering amplitude is the sum of three partial amplitudes illustrated on diagrams 1, 2, and 3.

tions of the two-body reaction

$$\pi^- p \rightarrow \pi^+ X,$$

where the mass M of X takes on the values indicated above.

Each box of Table II gives $(d\sigma/d\Omega)_K^*$ and its statistical error, and the average value of the emission angle θ^* of X.

The angular distributions of Table II are expanded in terms of Legendre polynomials $P_{L_1-1}(\cos\theta^*)$. The coefficients A_{L_1K} of the expansion

$$\left(\frac{d\sigma}{d\Omega}\right)_K^* = \sum_{L_1=1}^{6} A_{L_1K} P_{L_1-1}(\cos\theta^*),$$

as well as the quantity F ($F=\chi^2$/degrees of freedom), are given in Table III.

The total cross section, as deduced from our measurement of the reactions

$$\begin{aligned} \pi^- p &\rightarrow \pi^-\pi^+ n \\ &\rightarrow \pi^-\pi^+ n + m\pi^0 \qquad (m=1, 2, 3) \\ &\rightarrow \pi^-\pi^+ n + m(\pi^+\pi^-) \qquad (m=1, 2) \end{aligned}$$

is equal to 11.1±0.6 mb.

IV. THE MODEL

The model assumed by Deler and Valladas[2] and by Namyslowski *et al.*[5] is an extension of the model proposed by Lindenbaum and Sternheimer.[6] As was mentioned in the Introduction, they assume that the reaction takes place as a two-body reaction. Because there are three possible three-body final states, (1), (2), and (3), the amplitude describing the reaction can be written as the sum of three partial amplitudes schematized in Fig. 5.

One assumes that each diagram (i) can be written in the form of a product of two factors, where the first factor represents the production amplitude and the second represents the decay of the resonance considered.

A. Partial-Wave Expansion of the Transition Amplitude

The angular-momentum states of the reaction are defined as in Fig. 6, where L is the relative orbital angular momentum of the incident wave, L' is the relative orbital angular momentum of the pion π_1 and the subsystem $\pi_2 N$, l is the relative orbital angular momentum of the pion π_2 and the neutron ($l=1$ in the present case), and L'' is the relative orbital angular momentum of the neutron and the subsystem π_1-π_2.

An inelastic partial wave is defined by the sets (L,L',I,J) or (L,L'',I,J), where J is the total angular momentum and I is the total isospin.

For a given J, to each L' corresponds a single L''. Therefore, we shall label by a unique symbol N the partial waves having an isobar and those having a σ meson in their respective intermediate states. The expansion is limited to the partial waves $SD31$, $PP33$, $DD35$, $PP11$, $DS13$, $DD13$, $DD15$, and $FP15$, which correspond to the more absorbed partial waves, according to the partial-wave analysis of the elastic scattering.[1] In this notation, the first letter corresponds to the orbital angular momentum of the initial state, the second letter corresponds to the orbital angular momentum L' in the final state, the first number is equal to $2I$, and the second number is equal to $2J$.

The inelastic partial wave $PF33$ is neglected in favor of $PP33$ by considering the effect of the centrifugal barrier, and the wave $FF15$ is excluded by our experimental results (see Table III), which show that the coefficients A_{K6} are compatible with zero.

B. Transition Amplitude

Let $T_i(N)$ be the amplitude of the inelastic partial wave N where the subscript i refers to one of the three subsystems. One has

$$T_i(N) \propto T_i(W,W_i) f_i(N),$$

where the proportionality constant depends only on N,

$$T_i(W,W_i) = [(W_i - W_{ir}) + j\Gamma_i]^{-1},$$

$$f_i(N) = \sum_{m,\nu} a_m{}^{\nu}(N) P_{l_i}{}^{\nu}(\theta_i^*) Y_L{}^{m+\mu_i-\mu_f}(\theta,\phi),$$

where W_{ir} is the mass and Γ_i is the width of the resonance associated with the subsystem i; $j^2=-1$; W is the total energy in the over-all c.m. system; l_i is the relative orbital angular momentum of the particles of subsystem i; θ_i^* is the angle between the direction of either of the two particles of subsystem i and the direction of motion of subsystem i in the over-all c.m.

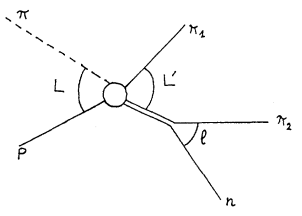

FIG. 6. Definition of the angular momentum states. L is the angular orbital momentum of the incident wave; L' is the relative orbital momentum between π_1 and the (π_2-N) system; l is the relative orbital momentum between π_2 and N.

[5] J. M. Namyslowski, M. S. K. Razmi, and R. G. Roberts, Phys. Rev. **157**, 1328 (1967).
[6] R. M. Sternheimer and S. J. Lindenbaum, Phys. Rev. **123**, 333 (1961).

TABLE IV. Values of the coefficients $X(N)$, where N is the inelastic partial wave index, obtained with and without π-π interaction.

Partial waves	$X(N)$ without $\pi\pi$ interaction ($B=0$)	$X(N)$ with $B=-0.58$
$PP33$	$(-0.3 \pm 0.03) + i(0.08 \pm 0.02)$	$(-0.3 \pm 0.04) - i(0.2 \pm 0.04)$
$SD31$	$(0.3 \pm 0.03) + i(0.94 \pm 0.13)$	$(-0.94 \pm 0.10) + i(0.3 \pm 0.04)$
$DD35$	$(-0.3 \pm 0.03) - i(0.40 \pm 0.06)$	$(0.6 \pm 0.06) - i(0.4 \pm 0.04)$
$PP11$	$(-0.6 \pm 0.06) + i(0.3 \pm 0.05)$	$(-0.2 \pm 0.04) - i(0.3 \pm 0.03)$
$DS13$	$(-0.2 \pm 0.02) + i(0.08 \pm 0.02)$	$(0.0 \pm 0.04) - i(0.2 \pm 0.04)$
$DD13$	$(0.4 \pm 0.05) + i(0.3 \pm 0.05)$	$(-0.4 \pm 0.04) - i(0.8 \pm 0.09)$
$DD15$	$(0.08 \pm 0.01) - i(0.1 \pm 0.02)$	$(0.4 \pm 0.05) + i(0.14 \pm 0.05)$
$FP15$	$(0.03 \pm 0.03) + i(0.2 \pm 0.03)$	$(-0.6 \pm 0.06) - i(0.04 \pm 0.04)$

system. This angle is measured in the rest frame of subsystem i. θ, ϕ are the polar angles of the incident pion direction in the reference system $\xi\eta\zeta$ of Ref. 2.

The transition amplitude is given by

$$\tau = \sum_N X(N)\{A(N)[T_1(N)+T_2(N)]+B(N)T_3(N)\},$$

where the summation is over the partial waves, and $A(N)$ and $B(N)$ are the relative contributions of the isobar and the dipion, respectively, in the partial wave N; $|A(N)|^2+|B(N)|^2=1$.

$X(N)$ is a complex number representing the relative weight of the wave N. In order to limit the number of parameters needed in our calculations, we shall assume that, for the partial waves of total isospin $I=\frac{1}{2}$, the coefficients $A(N)$ and $B(N)$ are real and independent of N. For the partial waves of total isospin $I=\frac{3}{2}$, $B(N)$ must be equal to zero.

The differential cross section $(d\sigma/d\Omega)_K^*$ then takes the following form for $K=1, 2, \cdots, 7$:

$$\left(\frac{d\sigma}{d\Omega}\right)_K^* (\text{computed}) = \sum_{L_1} \sum_{N,R} \text{Re}[X(N)X^\dagger(R)] \times C_{L_1K}'(W,N,R) P_{L_1}(\cos\theta_{\pi^- n}^*),$$

where N and R label the inelastic partial waves. The coefficients $C_{L_1K}'(W,N,R)$ are computed and do not contain any undetermined parameters except for the coefficients A and B. Setting

$$C_{L_1K}(W,W_1) = \sum_{N,R} \text{Re}[X(N)X^\dagger(R)] C_{L_1K}'(W,N,R),$$

the differential cross section $(d\sigma/d\Omega)_K^*$ becomes

$$\left(\frac{d\sigma}{d\Omega}\right)_K^* (\text{computed}) = \sum_{L_1} C_{L_1K}(W,W_1) P_{L_1}(\cos\theta_{\pi^- n}^*).$$

A similar expression is used to represent the experimental results;

$$\left(\frac{d\sigma}{d\Omega}\right)_K^* (\text{experimental}) = \sum_{L_1} A_{L_1K} P_{L_1}(\cos_{\pi^- n}^*),$$

where the coefficients A_{L_1K} (Table III) are determined by a least-squares method.

C. Comparison Method

The aim of this experiment is to determine the value of the complex coefficients $X(N)$, which are the relative weights of the partial waves N contributing to the reaction. These coefficients are obtained by comparing the calculated angular distributions $(d\sigma/d\Omega)^*$ to the corresponding measured distributions.

A least-squares method is used for this comparison. The function χ^2 is defined by

$$\chi^2 = \sum_{L_1K} \left[\frac{A_{L_1K} - C_{L_1K}'(X(N),A,B)}{\Delta A_{L_1K}}\right]^2,$$

when ΔA_{L_1K} = experimental error on A_{L_1K}.

The coefficients A and B are treated as fixed parameters, whereas the $X(N)$ are chosen by the program MINFUN in order to minimize the χ^2.

The quantity F, defined by

$$F = \chi^2/M,$$

where M is the number of degrees of freedom, is a measure of the goodness of a solution.

Neglecting the π-π interaction ($B=0$), the smallest value of F obtained is 1.7.

The value of F can be lowered by taking account of a π-π interaction. To do this, we have tried several values for the coefficients A and B ($B \neq 0$) and the smallest value of F obtained was 1.18, corresponding to $A=0.81$ and $B=-0.58$. Figure 7 shows the measured spectra as a function of the $(\pi^- n)$ system mass (Table I), as well as the calculated spectra (broken lines), at various angles where one assumes a π-π interaction ($F=1.18$). Table IV gives the coefficients $X(N)$ obtained with and without π-π interaction.

V. DISCUSSION

From Table IV, we notice that the coefficients of the waves $DD15$ and $FP15$ are small. This indicates that the D_{15} and F_{15} resonances are not strongly coupled to the channel $\Delta(1238)+\pi$. Furthermore, since F is fairly high ($F=1.7$) if one considers only this channel to describe the experimental results, one can suppose that these resonances also decay in one or several different channels.

The fit to the experimental angular distributions is improved by considering a π-π interaction. In this computation, the π-π resonance has a spin $J=0$ and an isospin $I=0$. The mass of this resonance is chosen to be $M=480$ MeV, together with a width Γ of 150 MeV. This resonance could be identified, with great caution, with the conjectured σ resonance, but one could equally well explain the data with a large π-π scattering length.

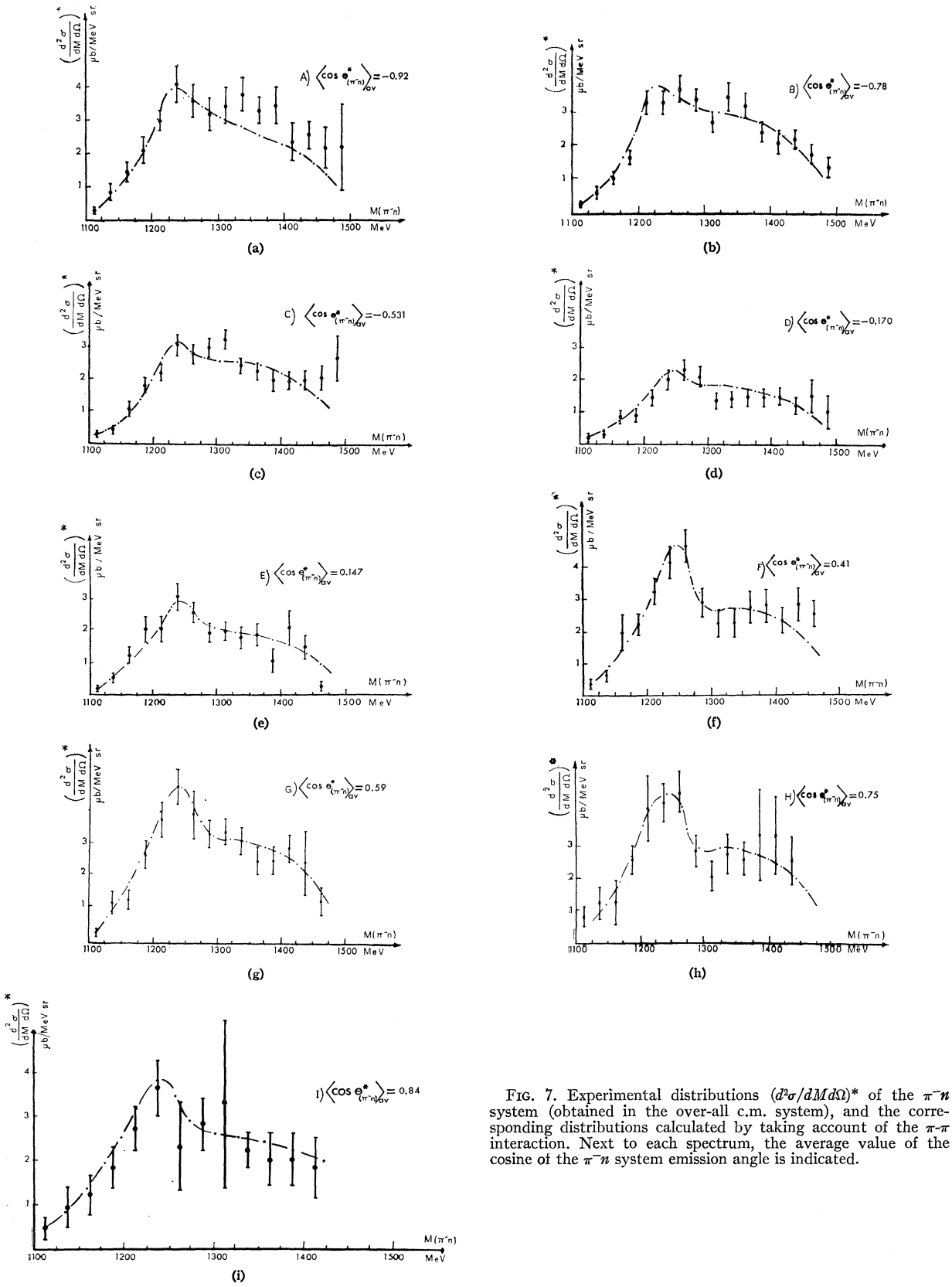

FIG. 7. Experimental distributions $(d^2\sigma/dMd\Omega)^*$ of the π^-n system (obtained in the over-all c.m. system), and the corresponding distributions calculated by taking account of the π-π interaction. Next to each spectrum, the average value of the cosine of the π^-n system emission angle is indicated.

In order to connect the coefficient $X(N)$ (in the case $B \neq 0$) to the absorption coefficients $(1-\rho_N^2)^{1/2}$ of the incoming waves, it is necessary to know also the coefficients $X(N)$ connected with the reactions $\pi^- p \to \pi^- p \pi^0$ and $\pi^- p \to \pi^0 \pi^0 n$. Thus, only when measurements in these channels become available will it be possible to determine the absorption coefficients by the study of the inelastic channels.

ACKNOWLEDGMENTS

We are very thankful to Dr. G. Valladas, Dr. B. Deler, and Dr. J. P. Merlo for fruitful discussions.

PHYSICAL REVIEW VOLUME 166, NUMBER 5 25 FEBRUARY 1968

Pion, Kaon, and Antiproton Production in the Center-of-Mass in High-Energy Proton-Proton Collisions*

L. G. RATNER
Particle Accelerator Division, Argonne National Laboratory, Argonne, Illinois

AND

K. W. EDWARDS†
Department of Physics, University of Iowa, Iowa City, Iowa

AND

C. W. AKERLOF, D. G. CRABB, J. L. DAY, A. D. KRISCH, AND M. T. LIN
Randall Laboratory of Physics, University of Michigan, Ann Arbor, Michigan

(Received 11 September 1967)

The differential production cross section $d^2\sigma/d\Omega dP$ has been measured for pions, kaons, and antiprotons produced in 12.5-GeV/c proton-proton collisions. In this experiment we studied the dependence of $d^2\sigma/d\Omega dP$ on the longitudinal and transverse components of the c.m. momenta of the produced particles, P_l and $P_\perp$, while holding all other variables fixed in the center-of-mass system. The ranges of the components measured were $P_l = 0.0$–1.0 GeV/c and $P_\perp^2 = 0.1$–1.5 (GeV/c)^2. The 12.5-GeV/c extracted proton beam of the Argonne ZGS impinged upon a liquid-hydrogen target. The produced particles were detected by a spectrometer containing two bending magnets and Čerenkov counters and scintillation counters in coincidence. The incident proton flux was determined by monitor scintillators calibrated during gold-foil irradiations. The cross sections for the production of $\pi^\pm$ and $K^\pm$ were all found to have an unambiguous Gaussian dependence on $P_\perp$ over the entire range. In the formula $d^2\sigma/d\Omega dP = B \exp(-AP_\perp^2)$, we found $A \approx 3.5$ (GeV/c)$^{-2}$ for $\pi^\pm$ and K^-. However, for K^+ we found $A \approx 2.7$ (GeV/c)$^{-2}$. In studying the dependence of $d^2\sigma/d\Omega dP$ on P_l, we found that the cross section was very strongly peaked about $P_l \approx 0.5$ GeV/c, with very few particles produced near $P_l = 0$. This shows that there is no tendency for particles to be produced at rest in the center-of-mass system. (Such production is predicted by the statistical model.) Instead, particles come out in two clouds or "fireballs" following the two departing baryons. These fireballs have a mass of about 2100 MeV.

1. INTRODUCTION

DURING the past few years there have been several "beam survey" experiments[1–5] performed at high-energy accelerators. In this type of experiment the differential production cross section $d^2\sigma/d\Omega dP$ for the production of secondary particles in high-energy proton-nucleus or proton-proton collisions was measured. These experiments were all done in the laboratory system, in that a series of measurements was made with θ_{lab} held fixed while P_{lab} was varied. The main purpose of these experiments was to obtain information to aid in the design of secondary particles. There were few serious attempts to relate these experimental data to the theory of strong interactions. The reason for the lack of theoretical interest in experiments of this type was that all these measurements were made in the laboratory system while it seems likely that any sensible theory of particle production in strong interactions will be simple only in the center-of-mass system.

* Supported by a research grant from the U. S. Atomic Energy Commission.

† Present address: Department of Physics, Carleton University, Ottawa, Canada.

[1] W. F. Baker, R. L. Cool, E. W. Jenkins, T. F. Kycia, S. J. Lindenbaum, W. A. Love, D. Luers, J. A. Niederer, S. Ozaki, A. L. Read, J. J. Russell, and L. C. L. Yuan, Phys. Rev. Letters **7**, 101 (1961).

[2] A. N. Diddens, W. Galbraith, E. Lillethun, G. Manning, A. G. Parham, A. E. Taylor, T. G. Walker, and A. M. Wetherell, Nuovo Cimento **31**, 961 (1964).

[3] D. Dekkers, J. A. Geibel, R. Mermod, G. Weber, T. R. Willitts, K. Winter, B. Jordan, M. Vivargent, N. M. King, and E. J. N. Wilson, Phys. Rev. **137**, B962 (1965).

[4] R. A. Lundy, T. B. Novey, D. D. Yovanovitch, and V. L. Telegdi, Phys. Rev. Letters **14**, 504 (1965).

[5] E. W. Anderson, E. J. Bleser, G. B. Collins, T. Fujii, J. Menes, F. Turkot, R. A. Carrigan, R. M. Edelstein, N. C. Hien, T. J. McMahon, and I. Nadelhaft, Phys. Rev. Letters **16**, 855 (1966); **19**, 198 (1967).

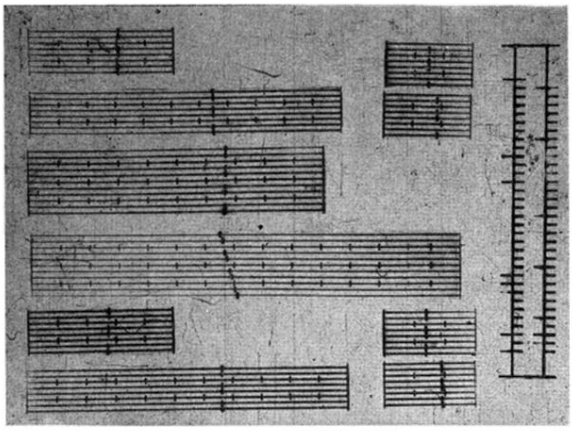

FIG. 2. Sample picture showing the data box and the fiducial marks followed by the flying spot.